Atmospheric Environment Vol. 27A, No. 9, pp. 1479–1490, 1993.
Printed in Great Britain.

0004–6981/93 $6.00 + 0.00

CALCULATION OF VISUAL RANGE IMPROVEMENTS FROM SO_2 EMISSION CONTROLS—II. AN APPLICATION TO THE EASTERN UNITED STATES

PAOLO ZANNETTI* IVAR TOMBACH† and SLAVKO CVENCEK
*AeroVironment, Inc., 825 Myrtle Avenue, Monorovia, CA 91016, U.S.A.

and

WILLIAM BALSON
Decision Focus. Inc., 650 Castro Street, Mountain view, CA 94041, U.S.A.

(*First received* 10 *March* 1989 *and in final form* 24 *November* 1992)

Abstract—This paper, the second of a two-part series, presents an application of a new semi-empirical methodology to assess the annual average improvements in visual range that can be expected from a reduction of SO_2 emissions in the eastern United States. This semi-empirical methodology was described in Part I of the series (Zannetti *et al.*, *Atmospheric Environment* **24A**, 2361–2368, 1990). As an illustrative example of its application, we calculate here the visibility improvements expected from a 12 million-tons yr^{-1} SO_2 emission reduction scenario (a reduction of about 55% from 1980 emissions) in the 31 eastern states. We find that a reduction of this size would generate improvements in visual range that, as regional annual averages over eight subregions throughout the eastern United States, vary from 8% (6; 11) to 11% (9; 15), where the two numbers between parentheses indicate "lower" and "upper" estimates, respectively, defined as plus/minus one standard deviation in a probability distribution. Thus, the relative visibility improvements are much smaller than the relative SO_2 emission reduction, with an "efficiency" (i.e. per cent visual range improvement divided by per cent emission reduction) that varies regionally from 0.15 (0.11; 0.20) to 0.21 (0.15; 0.28).

Key word index: Atmospheric visibility, sulfur, emission controls, visibility modeling, eastern United States.

1. INTRODUCTION AND SUMMARY

Anthropogenic sulfur dioxide (SO_2) emissions have been the main focus of attention as a cause of visibility degradation in the eastern United States because several investigations, such as summertime studies in Shenandoah National Park (Ferman *et al.*, 1981, Stevens *et al.*, 1984; Weiss *et al.*, 1982), have attributed a considerable fraction of the visibility impairment to ambient sulfate-containing particles. These particles are generated by atmospheric chemical reactions that oxidize the primary SO_2 emitted from anthropogenic sources into secondary sulfate (SO_4^{2-}). Several studies have attempted to quantify the role of such SO_2 emissions on visibility impairment and to evaluate the visibility improvements that could be expected from proposed SO_2 emission reduction. In particular, a draft report (SAI, 1984) prepared for the Environmental Protection Agency (EPA) estimated, using diffusion modeling techniques, the visibility improvements and their economic benefits related to several proposed SO_2 emission reduction scenarios. Subsequently, a further analysis of such potential improvements was presented by the same authors (Latimer and Hogo, 1987).

In performing benefit analyses of SO_2 emission reduction, it is critical to quantify correctly the "efficiency" of SO_2 controls on visibility impairment. For example, if a 50% reduction of SO_2 emissions in a control region $\mathscr{C}$ produces a 40% improvement in the average visual range in an impact region $\mathscr{I}$, we can say that the efficiency of that control scenario in that region is 0.8 (i.e. the ratio of 40 to 50). For a number of reasons that will be discussed throughout this report, annual average SO_2 control efficiencies may be as low as 0.15, with greater efficiencies for short-term episodes characterized by strong visibility impairment and high SO_4^{2-} ambient concentrations.

We have presented, in Part I (Zannetti *et al.*, 1990), a new semi-empirical methodology based on an intuitive mathematical approach that allows the calculation of the annual improvements in visual range that can be expected, in each region j during a meteorological regime k, from a reduction of SO_2 emissions. This approach expresses, in a fractional form, four separate effects: (1) the transport of atmospheric sulfur, de-

*Current address: Failure Analysis Associates, Inc., 149 Commonwealth Drive, P.O. Box 3015, Menlo Park, CA 94025, U.S.A.

†Current address: ENSR Consulting and Engineering, 1220 Avenida Acaso, Camarillo, CA 93012, U.S.A.

scribed by α_{jk}; (2) the non linearity β_{jk} of the SO_2-to-SO_4^{2-} transformation; (3) the sulfate fraction $\gamma_{jk}^{(w)}$ of fine particles; and (4) the fraction of light extinction that is due to fine particles, which is characterized by $\delta_{jk}^{(w)}$. Moreover, the method takes explicitly into account the roles of the water adsorbed by fine particles.

Part I dealt with the analytical description of the methodology. We present here an illustrative example of its application to the eastern United States, during the 3-year period 1979–81, a period characterized by no unusual meteorological conditions and relatively steady SO_2 emissions. The next section discusses the geography of the region and a subregional division of the eastern United States, Section 3 presents the state-by-state SO_2 emissions (E) and the selected emission control scenario (ΔE). Section 4 presents the criteria used for classifying the regional meteorology into suitable classes, which identify the major air mass transport scenarios in the East. The evaluation of the input data, i.e. the parameters α_{jk}, β_{jk}, $\gamma_{jk}^{(w)}$, $\delta_{jk}^{(w)}$ and their uncertainty, are described in Section 5, while Section 6 shows the outputs of our simulations and their uncertainty ranges. Finally, conclusions and future recommendations are presented in Section 7.

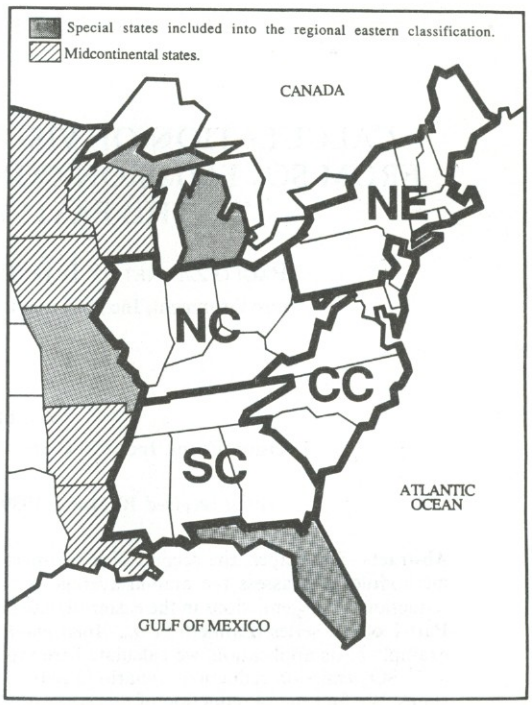

Fig. 1. Regional classification of the eastern United States: North East (NE), Coast Central (CC), North Central (NC), and South Central (SC).

2. THE SO_2 CONTROL REGION

The SO_2 control region $\mathscr{C}$ is shown in Fig. 1. It includes four areas (Northeast, North Central, Central Coast and South Central), five "midcontinental" states (Arkansas, Iowa, Louisiana, Minnesota and Wisconsin) and three states (Missouri, Michigan and Florida) whose special role will be discussed in Section 3. The emission scenario E was defined by using 1980 baseline emissions (SAI, 1984) in the region $\mathscr{C}$, while the control scenario ΔE was obtained by adjusting a 1995 31-state 13.1 million-tons*yr^{-1} (MTPY) SO_2 control scenario (SAI, 1984) to reflect 12 million-ton control scenario. Emission data are presented in Table 1.

3. THE IMPACT REGION

In this application of the method, the eastern United States were the impact region $\mathscr{I}$. More precisely, the region covered by the states below (26 states plus the District of Columbia) was divided into four impact areas (see Fig. 1):

1. Northeast (NE): Maine, Vermont, New Hampshire, Massachusetts, Connecticut, New York, Pennsylvania, Rhode Island;
2. North Central (NC): Illinois, Indiana, Ohio, Kentucky, West Virginia (with the addition† of Missouri and Michigan);
3. Central Coast (CC): New Jersey, Delaware, Maryland, Virginia, North Carolina, South Carolina (with the addition of the District of Columbia);
4. South Central (SC): Tennessee, Mississippi, Alabama, Georgia (with the addition† of Florida).

These four areas were further subdivided into urban and rural sections, resulting in eight subregions ($j=1,2,\ldots,8$). Naturally, the urban/rural differentiation does not affect the transport efficiency α and the chemical non-linearity β, since these parameters are based on the average regional meteorology, but it does not affect the sulfate fraction of fine particles (including water) $\gamma^{(w)}$, since this fraction is generally larger in rural areas (Shea and Auer, 1978; Mathai and Tombach, 1985; Noll *et al.*, 1985), and the fraction of light extinction due to fine particles $\delta^{(w)}$, since this function is generally lower in urban areas, where urban activities generate a relatively higher concentration of coarse particles.

*1 ton = 0.907 tonnes (metric tons).

†These states were added to avoid having states affected by major SO_2 controls outside the region $\mathscr{I}$. This would have created larger uncertainties in the determination of the boundary influx of sulfur. More precisely, the inclusion of these three states in $\mathscr{I}$ allows the incorporation of their emission controls into the fractional control terms $\Delta E_j/E_j$ (see Table 4) inside $\mathscr{I}$, instead of contributing to the terms $\Delta E_{j'}/E_{j'}$ outside $\mathscr{I}$. This assumption minimizes the uncertainties related to the problem of recirculation of air masses and determination of the contributions of the boundary conditions.

Table 1. SO_2 emission inventories and proposed controls for the eastern United States

Sequence No.	State	Region	EU80	NU80	TO80	SAI95	AV95
1	AL	SC	535	216	751	363	395
2	AK	*	27	75	102	133	130
3	CT	NE	29	40	69	79	78
4	DE	CC	51	57	108	61	65
5	DC	CC	0	10	10	7	7
6	FL	SC	692	369	1061	558	600
7	GA	SC	704	103	807	298	340
8	IL	NC	1110	345	1455	591	663
9	IN	NC	1672	468	2140	576	706
10	IA	*	236	97	333	132	149
11	KY	NC	1029	113	1142	261	334
12	LA	*	21	279	300	490	474
13	ME	NE	17	78	95	68	70
14	MD	CC	226	115	341	154	170
15	MA	NE	258	69	327	143	158
16	MI	NC	608	341	949	496	534
17	MN	*	160	83	243	159	166
18	MS	SC	122	156	278	212	217
19	MO	NC	1227	161	1388	281	373
20	NH	NE	80	12	92	23	29
21	NJ	CC	103	169	272	260	261
22	NY	NE	479	464	943	445	486
23	NC	CC	445	167	612	283	310
24	OH	NC	2185	475	2660	736	896
25	PA	NE	1422	556	1978	845	939
26	RI	NE	5	10	15	7	8
27	SC	CC	210	113	323	188	199
28	TN	SC	910	143	1053	288	352
29	VT	NE	0	6	6	6	6
30	VA	CC	158	197	355	195	208
31	WV	NC	984	144	1128	328	394
32	VVI	*	488	152	640	222	257
Total			16,193	5783	21,976	8888	9976

Values are in 10^3 tons yr^{-1} (=907 metric tons yr^{-1}).
EU80: electric utility SO_2 emissions for the 1980 baseline (from SAI, 1984); NU80: non-utility SO_2 emissions for the 1980 baseline (from SAI, 1984); TO80: EU80 plus NU80; SAI95: SAI 1995 31-State 13.1 million-ton control scenario (from SAI, 1984); AV95: SAI95 values adjusted to reflect a 12 million-ton control scenario.
* Midcontinental states.

4. METEOROLOGICAL CLASSIFICATION

We analysed the National Weather Service (NWS) daily weather maps from the 3-year period 1979–1981 for the eastern United States, and classified the air mass for each region and each day according to the standard meteorological classification described below. All days with midday relative humidity greater than or equal to 85% were placed in one class ($k=8$) that reflected times at which meteorology was likely to play a major role in visibility impairment through precipitation or fog. For relative humidity less than 85%, air mass transport classes ($k=1, 2, \ldots, 7$) were defined, similar to the classification of the Sulfate Regional Experiment (SURE) (Muller and Hidy, 1983). The eight classes are defined as follows:

$k=1$: cPk. Continental polar colder air, or cPk, is generally cool and dry. This class occurs most often during winter and in more northerly areas. Northerly winds usually dominate, with moderate to strong wind speeds. Precipitation may occur in the form of light snow or showers.

$k=2$: cPw. Following the high pressure zone cP2 (see below) in a normal progression comes the cPw, or continental polar warmed air. This air mass gives rise to slightly warmer temperatures and an increase in air stagnation as compared to the cPk condition. Winds become more moderate with occasional precipitation.

$k=3$: mT. When a continental high pressure cell has moved off the eastern coastline and amalgamated with the Bermuda high, it generates maritime tropical, or mT, conditions onshore. An increase in temperature and water content are strong characteristics of this air mass. Increased cloud cover with light to moderate onshore wind is also often associated with mT air.

$k=4$: Tr. A fourth class of air masses can be labeled transitional, or Tr, which includes a variety of cyclonic systems and mixed air masses with little temperature

and moisture homogeneity. Days when more than one air mass moved through an area were also included in this class.

$k=5$: cT. As maritime tropical air intrudes into the continent, the air mass obtains a continental tropical, or cT, condition. These are usually hot and dry continental air masses that occur most frequently in the summer. Light to moderate cloud cover with possible slight precipitation usually occurs under cT conditions.

$k=6$: cP2. Second in the western progression of anticyclones comes the standardized continental high pressure zone, cP2. This air mass, which occurs predominantly in the winter, is associated with light, variable winds and colder than average temperatures. Precipitation is infrequent and ventilation is usually poor.

$k=7$: mP. The maritime polar, mP, air mass originates over the North Atlantic. This air mass is characteristically cool and moist with a tendency, in winter, to become unstable. Heavy precipitation, low cloud cover and moderate winds generally occur under mP conditions.

$k=8$. All days with relative humidity greater than 85%.

Table 2 presents both the frequency of occurrence f_{jk} and the relative frequency of occurrence p_{jk} of each air mass transport class k in each region j during the 3-year period 1979–1981. The calculated frequencies show small variations between the urban and the rural values in the same region. This variation is due to the differences in relative humidity measured at urban and rural stations, which affect the number of days that have relative humidity above 85%.

Each meteorological regime has different significance for visibility. Among the several meteorological parameters affecting visibility (such as wind, temperature, humidity, solar radiation) the wind plays the major role. In fact, visual range will be relatively high under good ventilation conditions, but relatively low when stagnant conditions permit accumulation of pollution. Similarly, wind coming from relatively clean regions, such as the Atlantic Ocean, is generally associated with good visibility. Further information on visual range in the eastern United States under different meteorological regimes can be found in Zannetti *et al.* (1989).

Table 2. Frequency of occurrence f_{jk} and relative frequency of occurrence p_{jk} of each air mass transport class k for each region j

		$k=1$ cPk*		$k=2$ cPw		$k=3$ mT		$k=4$ Tr		$k=5$ cT		$k=6$ cP2		$k=7$ mp		$k=8$† RH > 85%	
j	Region	f	p	f	p	f	p	f	p	f	p	f	p	f	p	f	p
1	NE urban	342	0.321	135	0.127	121	0.144	163	0.153	19	0.018	67	0.063	147	0.318	71	0.066
2	NE rural	343	0.322	137	0.129	119	0.112	163	0.153	19	0.018	67	0.063	150	0.141	67	0.062
3	NC urban	359	0.337	262	0.246	38	0.036	174	0.163	77	0.072	79	0.074	27	0.025	49	0.047
4	NC rural	355	0.333	265	0.249	40	0.038	173	0.162	79	0.074	79	0.074	27	0.025	47	0.045
5	CC urban	144	0.135	118	0.111	298	0.280	203	0.191	43	0.040	42	0.039	157	0.147	60	0.057
6	CC rural	149	0.140	118	0.111	303	0.285	205	0.192	45	0.042	42	0.039	125	0.117	78	0.074
7	SC urban	123	0.115	137	0.129	417	0.392	202	0.190	57	0.054	37	0.035	19	0.018	73	0.067
8	SC rural	122	0.115	138	0.130	415	0.390	198	0.186	56	0.053	42	0.039	19	0.018	75	0.069

* See section 4 for definitions.
† All days with relative humidity > 85% are included in $k=8$.

5. ESTIMATES OF THE INPUT PARAMETERS

This section presents our estimates of the model parameters α_{jk}, β_{jk}, $\gamma_{jk}^{(w)}$ and $\delta_{jk}^{(w)}$ for the eastern United States, according to the methodologies discussed in Section I-3*. We assume that the probability distribu-

* The notation "I-#" is used throughout the paper to indicate a section or an equation in Part I paper (Zannetti *et al.*, 1990).

tion of each term is skewed and can be described by two half-Gaussian curves, with different standard deviations on the left and right side of the median. Moreover, for each j and k, the uncertainties in our estimates of α, β, $\gamma^{(w)}$ and $\delta^{(w)}$ are described by independent random variables with median values $\bar{\alpha}_{jk}$, $\bar{\beta}_{jk}$, $\bar{\gamma}_{jk}^{(w)}$, $\bar{\delta}_{jk}^{(w)}$ and standard deviations $\sigma_{\alpha_{jk}}^{+}$, $\sigma_{\beta_{jk}}^{+}$, $\sigma_{\gamma_{jk}}^{+}$, $\sigma_{\delta_{jk}}^{+}$ above the median and $\sigma_{\alpha_{jk}}^{-}$, $\sigma_{\beta_{jk}}^{-}$, $\sigma_{\gamma_{jk}}^{-}$, $\sigma_{\delta_{jk}}^{-}$ below the median.

The parameters α_{jk}, β_{jk}, $\gamma_{jk}^{(w)}$ and $\delta_{jk}^{(w)}$ below are computed only for $k=1, 2, \ldots 7$. In fact, for high relative humidity conditions (i.e. $k=8$), the visibility is impaired by natural phenomena and, consequently, negligible improvements in light extinction are expected from air quality improvements. Therefore, according to equation I-25, we assume $\delta_{j8}^{(w)} \simeq 0$ (i.e. $\theta_{j8}^{(w)} \simeq 0$, because, of equation I-8) for all the subregions j, and α_{j8}, β_{j8}, $\gamma_{j8}^{(w)}$ do not need to be computed.

5.1. *Estimates of α_{jk} and their uncertainty*

The terms α_{jk} are defined by equation I-3 and represent the "transport" efficiency of SO_2 emission controls on total sulfur concentrations in the subregion j under the kth meteorological regime. We estimated the median values $\bar{\alpha}_{jk}$ using the "intermediate" technique discussed in Section I-3.1, resulting in equation I-16, which was used with the following assumptions:

1. In each subregion j and under each meteorological regime k, total sulfur concentrations $(S)_{jk}$ are due 50% to local sources (i.e. in the same region, urban or rural), and 50% to the "upwind" region j'. This assumption gives $f_{jk}^{L}=f_{jk}^{D}=0.5$ in equation I-16.
2. The "upwind" region (or regions) j' was identified for each subregion j and meteorological class k, as presented in Table 3. These estimates are based on our evaluation of air mass trajectories. When two or three upwind regions were identified, the term $\Delta E_{j'}/E_{j'}$ was computed by averaging the contributions of these regions using their associated probabilities, which are shown in Table 3. These probabilities were computed either by using our expert judgment or by visually analysing geostrophic wind trajectories, using weather maps of selected days during the period 1979–81.
3. The total and regional fractional controls of SO_2 emissions ($\Delta E/E$, $\Delta E_{j'}E_{j}$ and $\Delta E_{j'}/E_{j'}$) were computed from the emission data in Table 1, as summarized in Table 4, and describe a 12 MTPY SO_2 emission reduction scenario.
4. For the regions j' outside the control region $\mathscr{C}$ (i.e. Canada and the Atlantic Ocean), we assumed a fixed value of $\Delta E_{j'}/E_{j'}=-0.05$ to represent the effect of decreased background sulfur concentrations as a consequence of the emission reduction. This choice of $\Delta E_{j'}/E_{j'}=-0.05$ for air masses coming from Canada and the Atlantic Ocean deserves some further discussion. In general, these air masses contain background sulfur concentrations due to natural sources and recirculation of anthropogenic sources. In most cases, these air masses are very "clean", since most of their sulfur has been deposited on the earth's surface. Therefore, SO_2 emission controls in the eastern United States will marginally affect the sulfur content of these air masses and $\Delta E_{j'}/E_{j'}$ will be very small. In some cases, however, air mass recirculation (e.g. from the eastern United States to the Atlantic Ocean and back to the eastern United States) is possible and could require higher values for $\Delta E_{j'}/E_{j'}$. The choice of $\Delta E_{j'}/E_{j'}=-0.05$ is an estimate between these extremes, which we believe is appropriate in most cases. We also carried out the complete analysis with a higher value of $\Delta E_{j'}/E_{j'}=-0.10$, and found

Table 3. Determinations of the "upwind" region (or regions) $j'(jk)$ for each of the four study regions and for each of the meteorological classes

j	Region	$k=1$ cPk	$k=2$ cPw	$k=3$ mT	$k=4$ Tr	$k=5$ cT	$k=6$ cP2*	$k=7$ mP
1 or 2	NE	(65) † NC (35)	NC (60) (40) †	NC (70) CC (30)	(60) † NC (40)	NC	NE (80) (20) †	
3 or 4	NC	(70) ‡ (30) †	(65) ‡ (35) †	(50) ‡ SC (50)	‡	‡	NC (80) (20) ‡	NE
5 or 6	CC	NC (65) SC (35)	NC (65) SC (35)	§	NC (50) SC (50)	NC (50) SC (50)	CC (80) NC (15) NE (5)	
7 or 8	SC	(65) ‡ NC (35)	(60) ‡ NC (40)	§	NC (50) (50) ‡	‡	SC (80) NC (15) (5) ‡	CC

When two or three upwind regions are indicated, their associated probabilities of occurrence (%) are also shown in parentheses.

* cP2 is associated with stagnant conditions and, therefore, the "upwind" region j' is equal to j.

† Air mass transported from Canada.

‡ Air mass transported from midcontinent states.

§ Air mass transported from the Atlantic Ocean.

Table 4. Estimates of fractional SO_2 controls

Region	j	Fractional control		Fractional control/($\Delta E/E$)
31-state		−0.55	(=$\Delta E/E$)	
NE	1 and 2	−0.50	(=$\Delta E_j/E_j$)	0.91
NC	3 and 4	−0.64		1.17
CC	5 and 6	−0.40		0.73
SC	7 and 8	−0.52		0.95
Midcontinental states	j'	−0.27	(=$\Delta E_{j'}/E_{j'}$)	0.50
Canada	j'	−0.05		0.09
Altantic Ocean	j'	−0.05		0.09

almost negligible variations in our results (see Section 6).

Under the assumptions and approximations above, equation I-16 gives a set of $\bar{\alpha}_{jk}$ values. This set is presented in Table 5. We believe that the uncertainty in this evaluation is high, due to uncertainty in the emission data and, especially, the air mass trajectories. Therefore, our estimates of the standard deviation of the error in estimating α_{jk} is one-fifth* of the interval between the minimum (0.41) and the maximum (1.11) $\bar{\alpha}_{jk}$ values in Table 5, i.e.

$$\sigma^{+}_{\alpha_{jk}} = \sigma^{-}_{\alpha_{jk}} = 0.15. \quad (1)$$

5.2. *Estimate of β_{jk} and their uncertainty*

The terms β_{jk} are defined by equation I-4 and represent the "non-linearity" of the SO_2-to-SO_4^{2-} transformation inside the air masses into which the controlled plumes are emitted. In other words, if an SO_2 emission is reduced by X%, the far downwind SO_4^{2-} concentration inside that air mass will decrease by βX%.

We applied the theoretical model results of Seigneur *et al.* (1984) to estimate the median values $\bar{\beta}_{jk}$ based on estimates of the cloudiness of each air mass k in region j. Relatively cloud-free skies were associated with $\bar{\beta}_{jk} = 1$ ("linear" chemistry), medium cloudiness with $\bar{\beta}_{jk} = 0.85$ and extensive cloudiness with $\bar{\beta}_{jk} = 0.70$. (Intermediate values were assigned to the Tr and cT air mass classes.) The estimated values of $\bar{\beta}_{jk}$ are presented in Table 6.

This evaluation is based on our expert judgement of a theoretical modeling analysis and, consequently, our evaluation of the standard deviation of the error in estimating β_{jk} is, again, one-fifth of the interval between the maximum (1.0) and minimum (0.7) values in Table 6, i.e.

$$\sigma^{+}_{\beta_{jk}} = \sigma^{-}_{\beta_{jk}} = 0.06. \quad (2)$$

For several β_{jk}, however, the standard deviations were reduced to force the $\bar{\beta}_{jk}$ value plus/minus two standard deviations to fall within the acceptable bounds for β, i.e. inside the interval 0.7–1.

5.3. *Estimate of $\gamma^{(w)}_{jk}$ and their uncertainty*

The terms $\gamma^{(w)}_{jk}$ are the sulfate fraction of fine particles, including the contribution of the adsorbed (or absorbed) water, according to equation I-17. We calculated the median values $\bar{\gamma}^{(w)}_{jk}$ using equation I-21 under the following assumptions:

1. The values of γ_{jk}, the sulfate fraction of fine particles as measured at low relative humidity, were computed using equations I-18 and I-19 with $\lambda = 1.25$, which represents an ammonium and sulfate mix consistent with measurements in the eastern United States (Mueller and Hidy, 1983).
2. Average sulfate anion (SO_4^{2-}) and fine particle mass (F) concentrations were computed, for each j and k, using data from the EPA Inhalable Particulate Monitoring Network. Values of γ/λ extracted from the few days in our data base with fine sulfate measurements are presented in Table 7. To provide a separate perspective on the γ/λ thus derived, we note that Mathai and Tombach (1985) evaluated the findings of five short-term eastern rural studies, all during summer, and estimated that 45% of the fine mass was SO_4^{2-}, i.e. in our notation, $\gamma/\lambda = 0.45$. In the one short-term summertime eastern urban study known to them (in Detroit, Wolff *et al.*, 1982) about 30–37% of the fine particulate matter mass was SO_4^{2-}, hence $\gamma/\lambda = 0.30$–0.37. Although these are short-term seasonal values, and results from only one urban study were available, these values of γ/λ compare resonably well with the average rural and urban estimates in Table 7. The annual values in the table are slightly lower than the summer values just cited because sulfates are typically a smaller fraction of the fine mass in other seasons than summer; similarly, the difference in γ/λ between the short-term summer rural and urban measurements is slightly greater than that seen in Table 7.
3. K_s, the sulfate "amplification" due to water adsorption, was computed using equation I-22 with RH_o

* Lacking better information, one-fifth of the range of a signal can be used, as a rule of thumb, to estimate its standard deviation.

Table 5. Evaluation of $\bar{\alpha}_{jk}$

j	Region	$k=1$ cPk	$k=2$ cPw	$k=3$ mT	$k=4$ Tr	$k=5$ cT	$k=6$ cP2	$k=7$ mP
1 and 2	NE	0.69	0.83	0.97	0.72	1.04	0.83	0.50
3 and 4	NC	0.78	0.77	0.95	0.84	0.84	1.11	1.04
5 and 6	CC	0.91	0.91	0.41	0.89	0.89	0.76	0.41
7 and 8	SC	0.84	0.86	0.52	0.89	0.72	0.95	0.84

Table 6. Evaluation of $\bar{\beta}_{jk}$

	$k=1$ cpK	$k=2$ cPw	$k=3$ mT	$k=4$ Tr	$k=5$ cT	$k=6$ cP2	$k=7$ mP
Any region j	0.85	0.85	0.70	0.75	0.80	1.00	0.70

Table 7. Values of γ/λ extracted from available Inhalable Particle Network data

j	Region	Maritime	Continental
1	NE urban	0.33	0.28
2	NE rural	0.37	0.30
3	NC urban	0.34	0.27
4	NC rural	0.35	0.27
5	CC urban	0.31	0.34
6	CC rural	0.35	0.35
7	SC urban	0.28	0.29
8	SC rural	0.35	0.30

$=0.4$, $\beta_s=1$ and $RH=(RH)_{jk}$, the average relative humidity at midday measured at three selected airports in each subregion j.*

4. K_{ns}, the "amplification" of nonsulfate fine particles due to water adsorption, was computed using equation I-23, with $RH=(RH)_{jk}$, $\beta_{ns}=1$ and $h_{ns}=0.5$, which indicates that 50% of the mass of nonsulfate species was assumed to be as hygroscopic as sulfate and the remaining 50% was assumed to be nonhygroscopic.

Under the assumptions and approximations above, a set of $\bar{\gamma}_{jk}^{(w)}$ values was computed. This set is presented in Table 8. These data, computed from a limited data base, seem to be about 10% lower than the data in the literature, which were collected mostly during episodic conditions. This fact, among other considerations, leads us to conclude that, using the data in Table 8 as "median" values for $\gamma_{jk}^{(w)}$, a skewed distribution can be assumed for the uncertainity on $\gamma_{jk}^{(w)}$. We chose an error standard deviation of 10% below the median and 20% above, i.e.

$$\sigma^{-}_{\bar{\gamma}_{jk}^{(w)}}=0.1\ \bar{\gamma}_{jk}^{(w)}, \tag{3}$$

and

$$\sigma^{+}_{\gamma_{jk}^{(w)}}=0.2\ \bar{\gamma}_{jk}^{(w)}. \tag{4}$$

5.4. *Estimate of $\delta_{jk}^{(W)}$ and their uncertainty*

The terms $\delta_{jk}^{(w)}$ represent the fraction of light extinction due to fine particles, including water, according to equation I-25. We calculated the median values $\bar{\delta}_{jk}^{(w)}$ in two ways. First, we used equations I-25 and I-26 with $\beta_f=1$, $RH_o=0.4$, $RH=(RH)_{jk}$, $F=(F)_{jk}$, and $e_f=3.1\ m^2\ g^{-1}$ for urban regions and $3.5\ m^2\ g^{-1}$ for rural regions. The e_f values were derived from Mathai and Tombach (1985), supplemented with additional recent data. Second, we performed, for each j and k, the linear regression of equation I-27 between the values $(LE)_{jk}^{(d)}$, computed from midday visual range measurements $(VR)_{jk}^{(d)}$ at airports, and $(F^{(w)})_{jk}^{(d)}$, computed using equation I-26, with $\beta_f=1$, $RH=(RH)_{jk}^{(d)}$ and $F=(F)_{jk}^{(d)}$. The superscript d ($d=1, 2, \ldots, N_{jk}$) indicates a day in which the air mass transport class k occurs in the subregion j. The regression provided the site-specific coefficients a_{jk} and b_{jk} that allowed the calculation of $\bar{\delta}_{jk}^{(w)}$ using equation I-28.

Both calculations, however, provided $\bar{\delta}_{jk}^{(w)}$ values smaller than we expected. In fact, since light extinction is mostly due to fine particles, we were expecting $\bar{\delta}_{jk}^{(w)}$ values in the range 0.80–0.95. Three possible explanations can be provided:

1. Airport measurements, because of limited targets at far distances, may systematically underestimate actual visual range thus overestimating the light extinction, i.e. the fraction of light extinction that is not attributed to fine particles. It is also possible that the Koschmieder scaling constant of 3.0 in equation I-1 may not properly represent the visual range vs extinction relationship.
2. Available aerosol measurements may underestimate the actual fine particle mass, because of loss of materials due to volatilization, thus increasing again the fraction of light extinction that cannot be associated with fine particles.

*Due to non-linearity of equation I-22, the use of $RH=(RH)_{jk}$ may underestimate the amplification factor K_s.

Table 8. Evaluation of $\bar{\gamma}_{jk}^{(w)}$

j	Region	$k=1$ cPk	$k=2$ cPw	$k=3$ mT	$k=4$ Tr	$k=5$ cT	$k=6$ cP2	$k=7$ mP
1	NE urban	0.35	0.37	0.43	0.42	0.36	0.38	0.44
2	NE rural	0.38	0.38	0.49	0.43	0.41	0.38	0.50
3	NC urban	0.37	0.36	0.44	0.40	0.37	0.34	0.49
4	NC rural	0.37	0.36	0.46	0.42	0.37	0.34	0.51
5	CC urban	0.42	0.42	0.43	0.45	0.43	0.42	0.42
6	CC rural	0.44	0.45	0.46	0.49	0.47	0.44	0.49
7	SC urban	0.37	0.37	0.37	0.38	0.39	0.37	0.36
8	SC rural	0.37	0.39	0.46	0.42	0.39	0.37	0.45

3. The role of other species (e.g. NO_2 and coarse particles) in visibility impairment may be greater than currently thought.

In spite of the above uncertainties, we used the two methods discussed above to calculate the final $\bar{\delta}_{jk}^{(w)}$, with the following assumptions:

1. When we trusted the linear regression (because of a high correlation coefficient and well-behaved scatter plots), we used the $\bar{\delta}_{jk}^{(w)}$ provided by the second method; when we did not, we used the results of the first method, or an average of the two.
2. To avoid unreasonably low values of $\bar{\delta}_{jk}^{(w)}$, a lower bound was used. We chose a minimum value of $\delta=0.6$ in urban areas and $\delta=0.7$ in rural areas. These lower bounds were based on our evaluations of the (quite limited) available data from the field studies analysed by Mathai and Tombach (1985) influenced by the noteworthy observation of Alkezweeny and Laulainen (1981) that fine mass accounted for only half of the light scattering aloft (above the inversion layer) in clean conditions over Lake Michigan and by several urban studies (not all in the East) that suggest carbon absorption in urban areas is 20% or more of extinction, vs a value closer to 10% in rural areas.
3. We also defined an upper bound for $\bar{\delta}_{jk}^{(w)}$ equal to $\delta=0.95$. This value was computed by considering the contribution of the Rayleigh scattering coefficient of the clean air, which at sea level has a value of $1.2\times10^{-5}\,m^{-1}$ for green light (Ruby and Waggoner, 1981).

Under the assumptions and approximations above, a set of $\bar{\delta}_{jk}^{(w)}$ values was computed. This set is presented in Table 9. Because of the lack of a solid database and the somewhat unclear results that we obtained from our regression analysis, we estimated the standard deviation of the error in $\bar{\delta}_{jk}^{(w)}$ to be quite high, at about 0.1, i.e.

$$\sigma^{+}_{\bar{\delta}_{jk}^{(w)}}=\sigma^{-}_{\bar{\delta}_{jk}^{(w)}}=0.1 \tag{5}$$

For several $\delta_{jk}^{(w)}$, however, this standard deviation was reduced to force the $\bar{\delta}_{jk}^{(w)}$ value plus/minus two standard deviations to fall within the acceptable bounds for $\delta^{(w)}$, i.e. inside the interval 0.6–0.95 in urban areas and 0.7–0.95 in rural areas.

6. RESULTS

The estimates of the probability distributions of α_{jk}, β_{jk}, $\gamma_{jk}^{(w)}$ and $\delta_{jk}^{(w)}$ presented in the previous section allow the application of the probability tree method described in Section I-4 and, consequently, the calculation of the probability functions $p(I_{jk}|\Delta E)$ of the visual range improvements I_{jk}. For example, the resulting probability distributions $p(I_{1,k}/\Delta E)$ for the seven ($k=1, 2, \ldots 7$) air mass categories for the NE urban region ($j=1$) are shown in Fig. 2.

As an example, we will follow the calculation of a single point in the probability tree. We calculate the fractional visual range improvement that results in the median (50th percentile) point for the cP2 air mass category ($k=6$) in the NE urban region ($j=1$), which is shown in Fig. 2. This point results from the median assumptions $\bar{\alpha}_{1,6}=0.83$, $\bar{\beta}_{1,6}=1$, $\bar{\gamma}_{1,6}^{(w)}=0.38$, $\bar{\delta}_{1,6}^{(w)}=0.75$ and the emission reduction fraction $\Delta E/E=-0.55$. Using equation I-7, we calculate the fractional change in light extinction to be -0.13 and, using equation I-9, we calculate the fractional change in visual range to be 0.15. The probability distribution in Fig. 2 reveals that this point occurs at the median for the cP2 air mass.

The curves in Fig. 2 provide ample evidence of why consideration of visibility improvements is clouded by uncertainty. The uncertainties in what happens under specific meteorological and atmospheric chemistry conditions produce dramatic variations in estimates of the visual range improvement that can be expected from one air mass category to another. For the cP2 air mass, which is associated with the largest improvements in visual range, the average annual fractional improvement of visual range has a median value of 0.15; there is a non-negligible probability of 10%, however, that the actual fractional improvement will be greater than 0.20 or (with the same probability of 10%) lower than 0.10. Similarly, for the mP air mass, which is associated with the smallest improvements in visual range, the average annual fractional improvement of visual range has a median value of 0.07; there is a 10% probability, however, that the actual value will be greater than 0.10 or (with the same probability) lower than 0.02. Note that daily improvements could be higher or lower than the values in the ranges shown here for the annual average.

Table 9. Evaluation of $\bar{\delta}_{jk}^{(w)}$

j	Region	$k=1$ cPk	$k=2$ cPw	$k=3$ mT	$k=4$ Tr	$k=5$ cT	$k=6$ cP2	$k=7$ mP
1	NE urban	0.60	0.62	0.75	0.61	0.60	0.75	0.75
2	NE rural	0.70	0.70	0.75	0.70	0.70	0.75	0.75
3	NE urban	0.73	0.65	0.85	0.62	0.73	0.60	0.92
4	NC rural	0.73	0.70	0.85	0.70	0.73	0.70	0.92
5	CC urban	0.60	0.60	0.67	0.61	0.60	0.60	0.60
6	CC rural	0.70	0.84	0.89	0.70	0.70	0.70	0.70
7	SC urban	0.67	0.61	0.85	0.90	0.60	0.60	0.92
8	SC rural	0.70	0.94	0.85	0.90	0.70	0.70	0.92

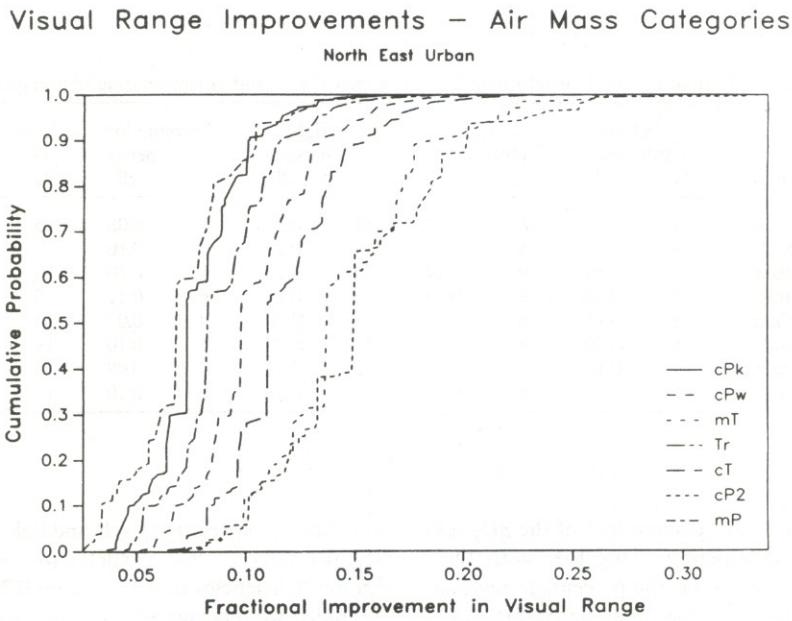

Fig. 2. Probability distributions $p(I_{1k}|\Delta E)$ of the visual range improvements I_{jk} in the northeast urban region for seven air mass transport cases (k . . 1, 2, . . . 7). Each probability is plotted in a cumulative form.

The probability distributions $p(I_{jk}|\Delta E)$ for all subregions j and meteorological regimes k are summarized in Table 10, which presents three points (16th, 50th and 84th percentiles*) of each distribution.

The "medium" values in Table 10 vary from 4 to 23%, the "low" values from 3 to 17% and the "high" values from 6 to 30%. The corresponding efficiencies of SO_2 emission reduction on visual range, i.e. per cent VR improvements divided by the average per cent SO_2 control (i.e. 55%), vary from 0.07 to 0.42 for the medium values, from 0.05 to 0.31 for the low values and from 0.13 to 0.55 for the high values. These efficiencies are much less than one, even though high efficiencies can be found in some regions during some meteorological regimes. The high values can be understood through analysis of the corresponding median values $\bar{\alpha}$, $\bar{\beta}$, $\bar{\gamma}^{(w)}$ and $\bar{\delta}^{(w)}$. For example, the maximum "medium" efficiency (0.23) is found for $j=4$ (NC rural) and $k=7$ (mP). The condition mP occurs in the NC region only 3% of the time (see Table 2). This high efficiency is due to the combination of a high transport efficiency with higher than average control upwind, giving a high $\bar{\alpha}_{4,7}(=1.04)$, a low $\bar{\beta}_{4,7}(=0.70$, i.e. strong nonlinearity), a high $\bar{\gamma}_{4,7}^{(w)}$ $(=0.51)$ and a very high $\bar{\delta}_{4,7}^{(w)}$ $(=0.92)$, reflecting that virtually all visibility impairment is caused by fine particles. Similar interpretations can be made for the other high values in Table 10.

In an analogous way, the probability tree method described in Section I-4 allows the calculation of the probability distributions $p(I_j|\Delta E)$ of the regional averages of the annual visual range improvements I_j, which are calculated using equation I-10 and the p_{jk} values shown in Table 2. Table 11 provides the 2nd,

* The 16th and 84th percentiles were chosen so that they correspond to the values of plus/minus one standard deviation when the distribution is normal.

Table 10. Medium visual range improvements I_{jk} as percentages (%)

j	Region	$k=1$ cPk	$k=2$ cPw	$k=3$ mT	$k=4$ tr	$k=5$ cT	$k=6$ cP2	$k=7$ mP
1	NE urban	7 [5,10]	10 [7, 13]	14 [11, 18]	8 [6, 11]	11 [9,15]	15 [11, 20]	7 [4, 9]
2	NE rural	9 [7, 13]	11 [9, 15]	16 [13, 21]	10 [7, 13]	15 [12, 20]	15 [11, 20]	8 [5,11]
3	NC urban	11 [8, 15]	9 [7, 12]	16 [12, 21]	9 [7, 13]	11 [8, 15]	14 [11, 19]	22 [17, 29]
4	NC rural	11 [8, 15]	10 [7, 13]	17 [13, 22]	11 [9, 15]	11 [8, 15]	17 [14, 23]	23 [17, 30]
5	CC urban	12 [9, 16]	12 [9, 16]	5 [3, 7]	11 [9, 15]	11 [9, 15]	12 [9, 16]	4 [3, 6]
6	CC rural	15 [12, 20]	19 [14, 25]	7 [4, 10]	14 [11, 19]	15 [11, 20]	15 [11, 20]	6 [4, 8]
7	SC urban	11 [8, 15]	10 [8, 13]	7 [5, 9]	14 [11, 19]	8 [6, 11]	13 [10, 18]	12 [9, 16]
8	SC rural	11 [9, 15]	17 [13, 23]	9 [6, 12]	16 [12, 21]	9 [7, 13]	16 [12, 21]	15 [12, 20]

Each value is the medium (580th percentile) as a percentage. Percentages in square brackets represent the 16th and 84th percentiles of I_{jk}.

Table 11. Annual regional visual range improvements I_j (%) and corresponding efficiencies

		Medium (50th perc.)		Low (16th perc.)		High (84th perc.)		Extreme low (2nd perc.)		Extreme high (98th perc.)	
j	Region	%	eff.	%	eff.	%	eff.	%	eff.	%	eff.
1	NE urban	8	0.15	6	0.12	11	0.21	4	0.08	15	0.27
2	NE rural	10	0.18	8	0.14	14	0.25	5	0.10	18	0.32
3	NC urban	10	0.19	8	0.14	14	0.26	6	0.10	18	0.33
4	NC rural	11	0.20	9	0.16	15	0.27	6	0.11	19	0.35
5	CC urban	8	0.15	6	0.11	11	0.20	4	0.07	14	0.26
6	CC rural	11	0.20	8	0.14	15	0.27	5	0.10	19	0.35
7	SC urban	9	0.16	7	0.12	12	0.22	4	0.08	16	0.28
8	SC rural	11	0.21	8	0.15	15	0.28	5	0.10	19	0.36

16th, 50th, 84th and 98th percentiles* of the $p(I_j/\Delta E)$ distributions for each region j, together with their corresponding efficiencies, i.e. the percentage regional improvement divided by the total percentage SO_2 control of 55%.

A comparison of the distributions shown in Table 11 reveals regional differences as would be expected. For example, the visual range improvements in the SC rural subregion are about 30% higher than those for the NE urban subregion, mostly because of the assessments of α, which represents the transport efficiency.

The medium regional efficiencies in Table 11 vary from 0.15 to 0.21, the low values from 0.11 to 0.16 and the high values from 0.20 to 0.28. Since we have included, in our error analysis, large uncertainties for the input parameters, we believe, to the best of our present knowledge, that the actual regional visual range efficiencies that we can expect from SO_2 controls are included within the ranges mentioned above.

The analysis of extreme cases in Table 11 shows a range from 0.07 to 0.11 for the low regional efficiencies and from 0.27 to 0.36 for the high regional efficiencies. To expand our understanding of possible extreme high efficiencies, we also computed, using the assumption of linear chemistry ($\beta=1$) and light extinction due virtually only to fine particles ($\delta^{(w)}=0.95$), median regional efficiencies that vary from 0.28 to 0.35.

Finally, we repeated the calculations using a larger sulfur "recirculation" assumption for the air masses coming from Canada and the Atlantic Ocean. This larger recirculation was performed by using the value of -0.1 instead of -0.05 for the upwind SO_2 controls $\Delta E_{j'}/E_{j'}$ (see Section 5.1). The impact of this assumption on the average regional efficiencies, however, was minimal (i.e. an increase of less than half per cent in the average regional improvements presented in Table 11). We conclude that, even under extreme assumptions, average regional efficiencies remain well below 0.40.

7. CONCLUSIONS AND RECOMMENDATIONS

This study provides an illustrative example of empirical evaluation of the visibility improvements that could be expected in the eastern United States as a consequence of the implementation of a large reduction of local SO_2 emissions. Our formulation emphasizes that four factors affect the expected visibility improvements:

1. Transport, since certain regions can be more or less affected by the SO_2 controls, depending upon air

* The 2nd and 98th percentiles were chosen so that they correspond to the values of plus/minus two standard deviations when the distribution is normal.

mass trajectories and the orientation of some receptor regions.
2. The possible nonlinearity of the SO_2-to-SO_4^{2-} reaction, which could cause a lower than expected reduction of SO_4^{2-} ambient concentrations.
3. The fact that sulfates are only a fraction of the visibility-impairing fine particles in the atmosphere.
4. The fact that fine particles are not the only cause of atmospheric visibility impairment.

Because of the combination of these four terms, the percentage improvements in visual range are much less than the percentage reduction of SO_2 emissions. The illustrative application of our approach to the eastern United States shows that a 12 MTPY SO_2 emission reduction scenario (a reduction of 55%) would generate average improvements of visual range in the eastern United States that vary from 8%, with an uncertainty range from 6 to 11% ($\pm$one standard deviation), to 11%, with an uncertainty range from 9 to 15%, depending on region. These numbers indicate that, under the particular assumptions used in our computations, the "efficiency" of SO_2 emission reduction on visual range (i.e. the percentage visual range improvement divided by the percentage emission reduction) varies from 0.15 (with an uncertainty range from 0.11 to 0.20) to 0.21 (with an uncertainty range from 0.15 to 0.28). Even under extreme assumptions, average regional efficiencies seem to remain well below 0.40.

Several steps in our calculations are based on expert judgments or semi-empirical assumptions because of the absence of data that quantify all input terms precisely. We have quantified estimated uncertainties, which, taken singularly, are quite large. Their combination, however, gives reasonable error bounds for our final visibility improvement calculations. Because our specification of input uncertainty was defined to reflect the full range of reasonably possible annual average values for the input parameters, we believe that all reasonably possible visual range improvements will lie within the ranges tabulated here.

Based on the investigations that we performed during this project and the results presented in the previous sections, it is clear that the available input data are inadequate to provide unchallengeable outputs. As a result, our method suffers from many of the problems associated with assembling a proper input for regional dispersion models. Accordingly, we have formulated research recommendations that aim at a better understanding of the effects of alternative pollution control scenarios on visibility in the eastern United States. To exploit fully the potential of this method, we encourage alternative evaluations of the parameters using models, data analysis, laboratory experiments and expert judgment evaluation by a panel of scientists. Our recommendations are the following:

1. Develop and use regional models for comparison and investigation, especially for a "modeling" evaluation of α_{jk}.
2. Conduct field, laboratory and theoretical research on the non-linearity of the SO_2-to-SO_4^{2-} transformation (i.e. evaluation of β_{jk}).
3. Conduct field experiments to provide more reliable databases for assessing the actual role of sulfates and other pollutants on visibility impairment in the eastern United States, as a function of the different meteorological regimes (i.e. evaluation of $\gamma_{jk}^{(w)}$ and $\delta_{jk}^{(w)}$ over long time periods as well as episodes).
4. In the interim, survey a large population of scientists for expert evaluation of the parameters, α, β, $\gamma^{(w)}$, and $\delta^{(w)}$ used in our methodology.

In order to understand better the implications of this method and to compare its performance with similar calculations by other methods, we engaged in an intercomparison of the semi-empirical method, regional dispersion modeling and the "transfer matrix" approach (e.g. Niemann, 1986) to extrapolating regional dispersion modeling results. The results of this intercomparison (Zannetti and Tombach, 1989) evaluated, to the extent feasible, the equivalents of the parameters α, β, γ, and δ for all methods to shed light on the reasons for any differences among them.

Acknowledgments—We thank Dr Prem Bhardwaja (Salt River Project) for his critical review and Dr William Wilson (U.S. EPA) for suggesting an improved treatment of the role of water than that in our first analyses. We extend our appreciation to Ms Wendy Webb for typing the manuscript and to Ms Anita Spiess for editorial review. This study was sponsored by the Utility Air Regulatory Group (UARG).

REFERENCES

Alkezweeny A. J. and Laulainen N. S. (1981) Comparison between polluted and clean air masses over Lake Michigan. *J. appl. Met.* **20,** 209–212.

Ferman M. A., Wolff G. T. and Kelly N. A. (1981) The nature and sources of haze in the Shenandoah Valley/Blue Ridge Mountain Area. *J. Air Pollut. Control Ass.* **31,** 1074–1081.

Latimer D. A. and Hogo H. (1987) The relationship between SO_2 emissions and regional visibility in the eastern United States. In *APCA Specialty Conference, Visibility Protection: Research and Policy Aspects.* Grand Teton National Park, Wyoming, September 1986.

Mathai C. V. and Tombach I. H. (1985) Assessment of the technical basis regarding regional haze and visibility impairment. AeroVironment Report AV-FR-84/420.

Mueller P. K. and Hidy G. M. (1983) The Sulfate Regional Experiment: report of findings. Electric Power Research Institute Report EA-1901, Palo Alto, California.

Niemann B. L. (1986) Regional acid deposition calculations with the IBM PC LOTUS 1-2-3 system. *Envir. Software* **1,** 175–181.

Noll K. E., Pontius A., Frey R. and Gould M. (1985) Comparison of atmospheric coarse particles at an urban and nonurban site. *Atmospheric. Environment* **19,** 1931–1943.

Ruby M. G. and Waggoner A. P. (1981) Intercomparison of integrating nephelometer measurements. *Envir. Sci. Technol.* **15,** 109–113.

Seigneur C., Saxena P. and Roth P. M. (1984) Computer simulations of the atmospheric chemistry of sulfate and nitrate formation. *Science* **225,** 1028–1030.

Shea D. M. and Auer Jr A. H. (1978) Thermodynamic properties and aerosol patterns in the plume downwind of St. Louis, *J. appl. Met.* **17,** 689–698.

Stevens R. K., Dzubay T. G., Lewis C. W. and Shaw R. W. (1984) Source apportionment methods applied to the determination of the origin of ambient aerosols that affect visibility in forested areas. *Atmospheric Environment* **18,** 261–272.

Systems Applications, Inc. (SAI) (1984) Visibility and other air quality benefits of sulfur dioxide emission controls in the eastern United States. Draft report SYSAPP-84/165.

Weiss R. W., Larson T. V. and Waggoner A. P. (1982) In situ rapid-response measurement of $H_2SO_4/(NH_4)_2SO_4$ aerosols in rural Virginia. *Envir. Sci. Technol.* **16,** 525–532.

Wolff G. T., Ferman M. A., Kelley N. A., Stroup D. P. and Rathkosky M. S. (1982) The relationships between the chemical composition of fine particles and visibility in the Detroit metropolitan area. *J. Air Pollut. Control Ass.* **32,** 1216–1220.

Wolff G. T., Kelley N. A., Ferman M. A., Rathkosky M. S., Stroup D. P. and Korsog P. E. (1986) Measurements of sulfur oxides, nitrogen oxides, haze and fine particles at a rural site on the Atlantic Coast. *J. Air Pollut. Control Ass.* **36,** 585–591.

Zannetti P. and Tombach I. (1989) Intercomparison of numerical techniques for the simulation of visibility improvements from SO_2 emission controls in the eastern United States. In *Proceedings, AWMA/AMS Specialty Conference on Visibility and Fine Particles.* Estes Park, Colorado, October.

Zannetti P., Tombach I. and Cvencek S. (1989) An analysis of visual range in the eastern United States under different meteorological regimes. *J. Air Pollut. Control Ass.* **39,** 200–203.

Zannetti P., Tombach I. and Balson W. (1990) Calculation of visual range improvements from SO_2 emission controls—I. Semi-empirical methodology. *Atmospheric Environment.* **24A,** 2361–2368.